Hyperons at the BM@N experiment: first results

Julia Gornaya[2,], *Mikhail* Kapishin[1], *Vasiliy* Plotnikov[1], *Gleb* Pokatashkin[1,*], *Igor* Rufanov[1], *Veronica* Vasendina[1], and *Alexander* Zinchenko[1]

[1]Joint Institute for Nuclear Research (JINR), Dubna, Russia
[2]National Research Nuclear University (MEPhI), Moscow, Russia

Abstract.
BM@N (Baryonic Matter at Nuclotron) is the first experiment to be realized at the accelerator complex of NICA-Nuclotron at JINR (Dubna). The aim of the experiment is to study interactions of relativistic heavy ion beams of kinetic energy per nucleon ranging from 1 to 4.5 GeV with fixed targets. First results of the analysis of minimum bias interactions of the deuteron and carbon beams of 4 AGeV kinetic energy with different targets are discussed. Preliminary results from the data collected in the recent experimental run with the argon beam are also presented.

1 Introduction

The Baryonic Matter at Nuclotron (BM@N) is a new experiment designed to investigate properties of dense nuclear matter in nucleus-nucleus collisions. The newly constructed accelerator complex of NICA-Nuclotron will provide several kinds of heavy ion beams up to gold of the kinetic energy from 1 to 4.5 AGeV and intensity up to 10^7 per second. The Nuclotron beam energy range is appropriate to study strange and multi-strange particles such as Λ, Ξ, Ω produced close to the kinematic threshold. The production yields of (anti-) hyperons and strange mesons measured in different experiments are shown in Fig. 1 (left). In heavy ion collisions strange hadrons can coalesce with light nuclear fragments and form hypernuclei [1, 2]. Fig. 1 (right) shows the yields of hypernuclei as predicted by the thermal model [3]. The maximum in the hypernuclei production rate is predicted at $\sqrt{S_{NN}} \sim$ 4-5 GeV, which is close to the Nuclotron beam energy range. Studies of hypernuclei production processes are expected to provide insight into the properties of the hyperon-nucleon and hyperon-hyperon interactions.

In the latest three years the BM@N experiment recorded experimental data with the deuteron, carbon, argon and krypton beams. The first methodical paper describing Λ^0-hyperon reconstruction in interactions of the deuteron beam with different targets (December 2016) is published [4]. The paper also gives a description of the data analysis methods such as the detector alignment and Lorentz shift correction, primary vertex reconstruction and technical details of the central tracker such as the spatial and momentum resolution.

In the latest experimental run performed in March 2018 the research program included the measurement of inelastic reactions of the argon and krypton beams with various targets. In particular, the measurement was focused on hyperon reconstruction in the central tracker,

*e-mail: pokat@jinr.ru

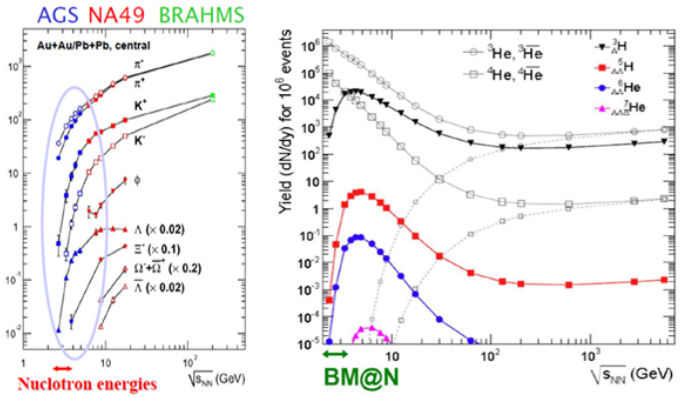

Figure 1. Left plot: Yields of mesons and (anti-) hyperons measured in different experiments as a function of the energy per nucleon- nucleon collision in c.m.s. for Au+Au and Pb+Pb collisions [5]. The Nuclotron beam energy range corresponds to $\sqrt{S_{NN}}$= 2.3 - 3.5 GeV. Right plot: Yields of hypernuclei predicted by the thermal model [3] for Au+Au collisions as a function of the nucleon-nucleon collision energy in c.m.s. Predictions for the yields of ^3He and ^4He nuclei are presented for comparison. The Nuclotron BM@N energy range is specified

identification of charged particles and nuclear fragments with the time-of-flight system, reconstruction of γ and multi-γ states with the electromagnetic calorimeter. A separated run of the BM@N experiment performed in the carbon beam with the liquid H_2 target was devoted to studies of short-range correlations (SRC) [6].

2 Detector geometry

2.1 Conceptual detector setup

A sketch of the BM@N setup is shown in Fig. 2. The detailed description of the BM@N geometry can be found in [7]. The basic detector setup comprises the central tracker inside the analyzing magnet (forward silicon detectors and GEM detectors), outer tracker based on drift chambers (DCH) and cathode strip chambers (CSC), electro-magnetic calorimeter behind the magnet, two time-of-flight detectors (mRPC-1 and mRPC-2), zero degree calorimeter (ZDC), start T0 and trigger detectors around the target.

The main advantage of the setup is a large aperture analyzing magnet with 1 m gap between the poles. The magnet aperture is filled with coordinate detectors which sustain high multiplicities of particles and are operational in the strong magnetic field. Two walls of time-of-flight detectors placed "near to magnet" and "far from magnet" serve to identify particles with a low and high momentum. The link between the central tracker and time-of-flight detectors is done by the outer tracker.

2.2 Central tracker

The central tracker of the BM@N experiment is based on two-coordinate triple Gas Electron Multipliers (GEM) [8]. The GEM detectors have the established technology developed at the CERN workshop and have been used in various experiments (COMPASS, JLAB, STAR, CMS).

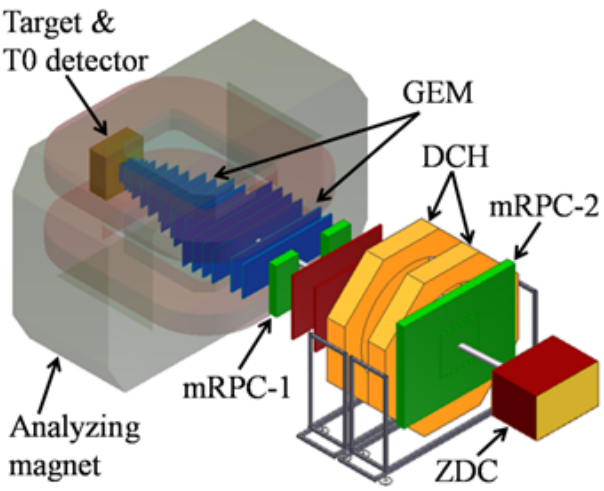

Figure 2. Schematic view of the BM@N setup

Based on the analysis of the experimental data collected in the deuteron run, the central tracker was extended with two-coordinate planes of a forward silicon detector designed to improve the primary vertex reconstruction [9]. One silicon plane was operated in the carbon run (March 2017), two extra silicon planes were installed in the latest run with the argon and krypton beams in March 2018. The GEM tracker was upgraded to six large area detectors. The central tracker configuration was tuned to measure soft decay products of strange V0 particles. The positions of the GEM and silicon detectors were optimized using Monte-Carlo simulation. The central tracker configurations in the recent runs are shown in Fig. 3.

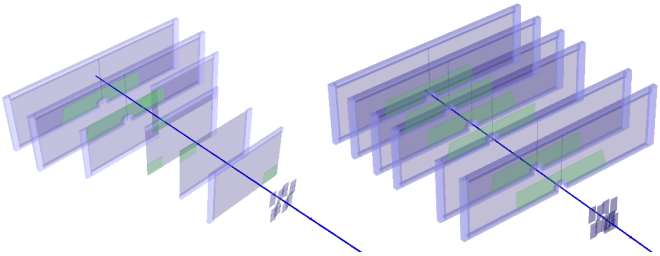

Figure 3. Left plot: BM@N setup used in the carbon run. Right plot: BM@N setup used in the Ar/Kr run

3 Event reconstruction and Monte-Carlo simulation

The track reconstruction method was based on a so-called "cellular automaton" approach [10]. The tracks found were used to reconstruct primary and secondary vertices using the "KFparticle" formalism [11]. In fact, both (track and vertex) reconstruction packages were adapted from the CbmRoot software framework [12], where they were used very extensively for Monte-Carlo studies of the Silicon Tracking System (STS) of the CBM detector performance. Due to rather similar detector configurations, the synergetic approach to the software

development was quite natural to follow. It allowed us to reduce significantly the development time and efforts. To test the quality of the event reconstruction procedure and confirm our understanding of the detector operation features, the "realistic" Monte-Carlo simulation of the spectrometer response was performed. The event samples of $C+A$ collisions were produced with the DCM-QGSM event generator [13–16]. The passage of particles through the setup volume was simulated with the GEANT package integrated into the BmnRoot software framework [17]. To describe the GEM detector response in the magnetic field, the microsimulation package Garfield++ [18] was used. The package gives a very detailed description of the processes inside the GEM detector, including the drift and diffusion of ionization electrons in the electric and magnetic fields and the electron multiplication in the GEM foils, so that the output signal from the readout plane can be reproduced. To speed up the simulation, the parameterization of the Lorentz shifts of electrons and the charge distributions on the readout planes was done as a function of the drift distance and used in the GEM digitization part of the BmnRoot package. The level of agreement of the experimental and simulated results can be seen below.

4 Results and discussion

Some analysis results for the experimental data collected in the carbon and argon beams are presented below.

4.1 Primary vertex reconstruction

Fig. 4 shows distributions of the primary vertex along the beam (Z-coordinate) reconstructed in the carbon and argon runs with different targets positions: at -24 cm for the carbon run and at 0.6 cm for the argon run. One can see that the resolution obtained for the argon beam is better because of a higher track multiplicity, a better detector coordinate resolution (in particular, due to additional silicon detector planes) and a smaller distance from the target to the first detector station. The reconstructed experimental Z-coordinate distribution width ($\sigma \simeq 0.6$ cm) for the C+Al interaction vertices was well reproduced by the simulation.

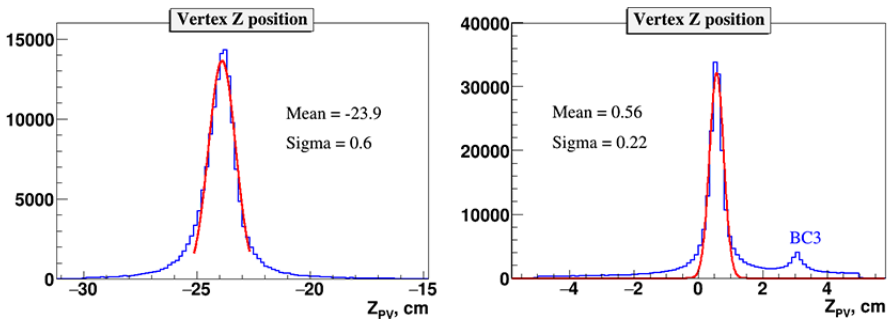

Figure 4. Reconstructed primary vertex along the beam: left) C + Al interactions, right) Ar + Al interactions. The small bump in the Ar-beam distribution is due to interactions in the trigger counter BC3

4.2 Beam momentum determination

The experimental data without a target were collected to measure the carbon beam momentum in the central tracker located in the magnetic field of 0.6 T. Since the carbon ionization is 36

times as large as that of deuteron, the high voltage applied to GEM detectors has been reduced in order to fit the electronics dynamic range for the output signal.

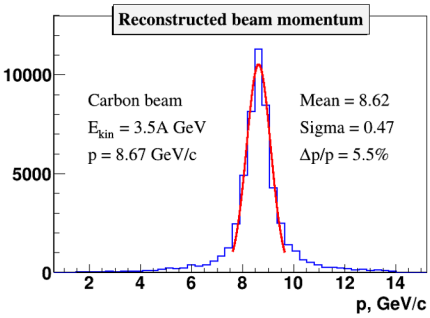

Figure 5. Carbon beam rigidity measured in the central tracker

The momentum distribution for the reconstructed carbon beam particles with a rigidity of p/q of 8.67 GeV/c is shown in Fig. 5. Here p is the beam particle momentum and q is its charge. It is this value that is measured in any magnetic spectrometer. The obtained beam rigidity resolution is $\sim$ 5.5%. The momentum resolution for the reconstructed tracks produced in interactions (like protons or π^--mesons) should be much better because their momenta are lower than the beam particle momentum and their trajectories have larger curvatures.

4.3 Comparison with Monte-Carlo simulation

The MC simulation has been tuned to reproduce experimental data on interactions of the carbon beam with the targets to evaluate the detector efficiencies and understand better the detector response. Nucleus-nucleus interactions were generated by using the DCM-QGSM model [13–16]. As mentioned above, the GEM detector effects (Lorentz shifts) were included into the detector response simulation part. In addition, the detector efficiency in the simulation was adjusted to reproduce results on the hit multiplicity distribution for the reconstructed tracks. As it can be seen from the two-dimensional distributions of the hit residuals with respect to the found tracks in GEM detectors versus hit coordinates (Fig. 6), the observed pattern can be described in general by the simulation except in the beam area, where the experimental data demonstrate excessive broadening due to the effect of the pile-up from beam particles, which has not been included in the simulation yet.

The current status of the momentum spectra agreement is shown in Fig. 7. One can see that the experimental momentum spectrum is reasonably reproduced in the simulated events aside from the momentum range of spectator protons around 3.5-5.5 GeV/c. This can be attributed to the GEM detector performance deterioration in the beam maximum area.

The transverse momentum distributions demonstrate a similar level of agreement (Fig. 8), i.e. negative particles are better described by the simulation, and somewhat harder p_T-spectrum of positive tracks can be also explained by the lack of the reconstructed proton spectators in the experimental data.

4.4 Λ^0 and K_s^0 reconstruction

Λ^0-hyperons were reconstructed using their decay mode into proton and π^-. The signal event topology (decay of a relatively long-lived particle into two tracks) defined the selection

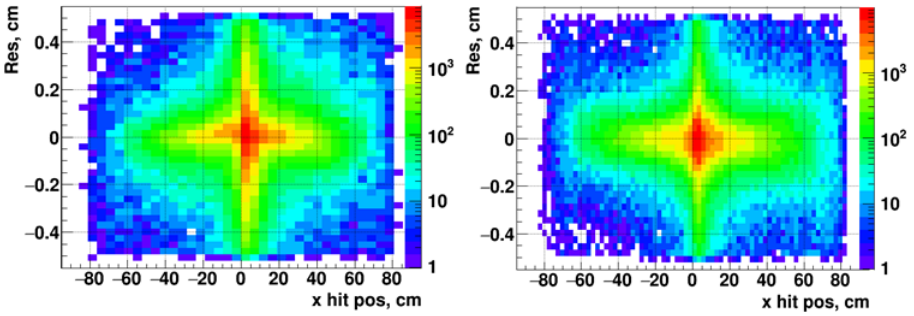

Figure 6. The x-coordinate residuals of hits with respect to tracks as a function of hit x-positions in the GEM detector: left) for carbon data, right) for simulated tracks

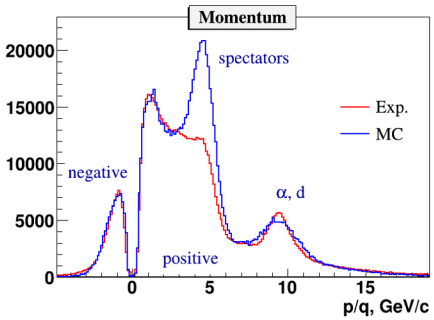

Figure 7. Comparison of momentum distributions for the negative and positive particles reconstructed in the experimental data and MC

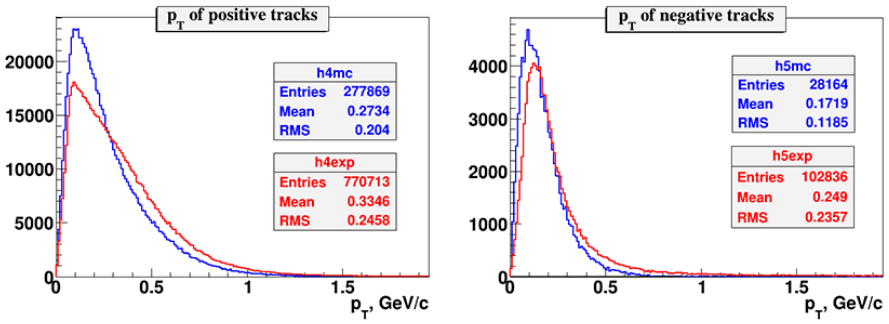

Figure 8. Particle transverse momentum distributions for data and simulation: (left) for positive tracks, (right) for negative tracks

criteria: a relatively large distance of the closest approach (DCA) of decay products to the primary vertex, poor track-to-track separation in the decay vertex, a relatively large decay length of the mother particle. Since the particle identification was not used at this stage of the analysis, all the positive tracks were considered as protons (π^+ for K^0_s) and all the negative

tracks as π^-. In Fig. 9 one can see the reconstructed topology of Λ^0 decay with the tracks originated from the secondary and primary vertices.

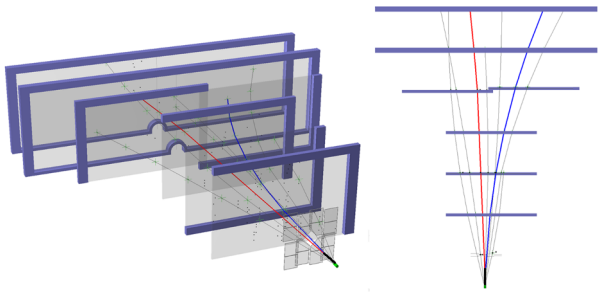

Figure 9. Example of the Λ^0 decay reconstructed in the central tracker in C+C interaction. The red line is a positive track (proton), the blue line is a negative track (π^-), the black line is a combined track (Λ^0), the green line is a reconstructed vertex. Left) Perspective view of the reconstructed event in the central tracker; Right) Top view of the reconstructed event in the central tracker

The data samples collected with 3 targets (C, Al, Cu) were analyzed to reconstruct Λ^0-hyperons and K_s^0 in the carbon run. The obtained invariant mass distribution of proton, π^- pairs is shown on the left plot in Fig. 10. The π^+, π^- invariant mass spectrum is shown on the right plot. One can see the Λ^0-peak with σ ~2.8 MeV. The significance of the K_s^0 reconstructed peak on the right plot of Fig. 10 is not very high. It can be explained by the fact that the central tracker configuration was tuned to measure relatively high-momentum beam particles, and the geometric acceptance for relatively soft decay products of strange V0 particles was rather low. The Monte-Carlo simulation has shown that only ~ 4% of Λ^0 and ~ 0.8% of K_s^0 could be reconstructed.

The kinematic reflection of $K_s^0 \rightarrow \pi^+\pi^-$ decay into the (p,π^-) effective mass spectrum contributes to (p,π^-) masses higher (around 1209 MeV) than the Λ^0 hyperon one of 1115.6 MeV and does not mimic the Λ^0 hyperon signal. Vice versa, the kinematic reflection of $\Lambda^0 \rightarrow p\pi^-$ decay contributes to the lower masses (around 344 MeV) in ($\pi^+\pi^-$) effective mass spectra than K_s^0 mass of 498 MeV and is not mixed with the $K_s^0 \rightarrow \pi^+\pi^-$ signal. In the Lambda reconstruction the algorithm candidates to protons are selected with a much higher momentum than candidates to π^-. This requirement eliminates the background from π^+ among the proton candidates.

A "first look" result on the invariant mass spectrum of proton-π^- pairs reconstructed in interactions of the argon beam with targets is shown in Fig. 11. The result was obtained on a small fraction of the collected statistics and without dedicated tuning of the track reconstruction algorithm.

5 Summary and plans

The BM@N experiment is in the starting phase of its operation and has recorded experimental data on interactions of the carbon, argon and krypton beams of several energies with different targets. Experimental data of minimum bias interactions of the carbon beam with different targets have been analyzed to reconstruct tracks, primary and secondary vertices using the central tracking detectors. The signals of Λ^0-hyperon and K_s^0 were reconstructed in the invariant mass spectra of particles originated from secondary vertices. To improve the vertex and momentum resolution and reduce the background under the Λ^0-hyperon signal,

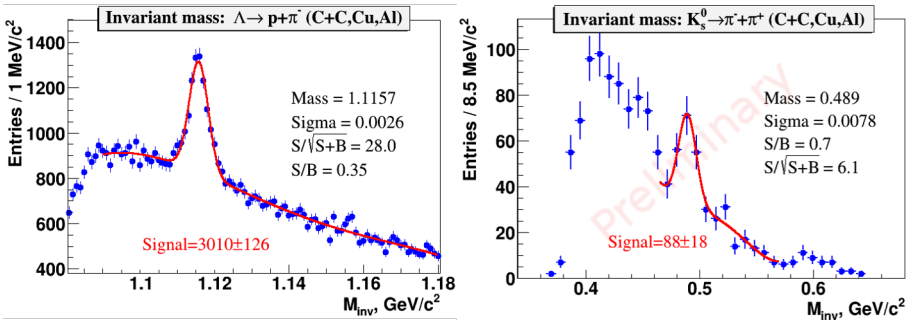

Figure 10. Left) Invariant mass spectrum of proton+π^- pairs, Right) Invariant mass spectrum of $\pi^+ + \pi^-$ pairs

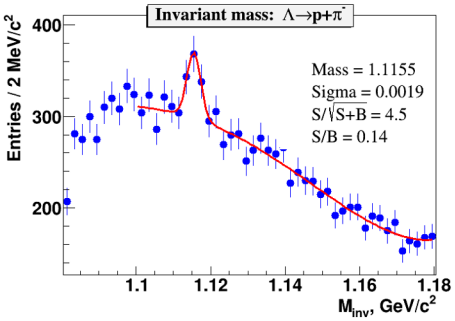

Figure 11. Invariant mass spectrum of proton+π^- pairs reconstructed in interactions of the argon beam with targets

two extra silicon planes have been installed into the central tracker. The BM@N setup will be extended to the full configuration to adapt its performance for measuring the interactions of heavier ion beams with targets. The work is ongoing to tune the Monte Carlo simulation to describe the experimental data for obtaining Λ^0-hyperon yields.

Acknowledgments. This work was partially supported by the Ministry of Science and Education of the Russian Federation, grant N 3.3380.2017/4.6, and by the National Research Nuclear University MEPhI in the framework of the Russian Academic Excellence Project (contract No. 02.a03.21.0005, 27.08.2013).

References

[1] J. Steinheimer, H. Stoecker, I. Augustin, A. Andronic, T. Saito and P. Senger, Prog. Part. Nucl. Phys. **62**, 313 (2009)
[2] J. Steinheimer, K. Gudima, A. Botvina, I. Mishustin, M. Bleicher and H. Stocker, Phys. Lett. B. **714**, 85 (2012)
[3] C. Blume, J. Phys. G **S57**, 31 (2005)
[4] D. Baranov et. al (BM@N Collaboration), PEPAN Letters **15**(2), 148-156 (2018)
[5] A. Andronic et al., Phys. Lett. B **695**, 203 (2011)
[6] *Probing Short Range Correlations BM@N Project*, http://bmnshift.jinr.ru/wiki/lib/exe/fetch.php?media=proposal_bmn_dubna_final.pdf

[7] *BM@N Project report*,
http://bmnshift.jinr.ru/wiki/lib/exe/fetch.php?media=bmnproject_2016.pdf
[8] *BM@N Technical Design Report for the GEM Tracking System*,
http://bmnshift.jinr.ru/wiki/lib/exe/fetch.php?media=tdr_gem_may2017_v1.doc
[9] N. Zamiatin, *Status of Silicon Detector for next Run*,
http://bmnshift.jinr.ru/wiki/lib/exe/fetch.php?media=sildet_bm_n_21.12.17.ppt
[10] V. Akishina, I. Kisel, J. Phys.: Conf. Ser. **599**, 012024 (2015)
[11] S. Gorbunov, I. Kisel, *Reconstruction of decayed particles based on the Kalman filter*, CBM-SOFT-note-2007-003 (2007)
[12] http://cbmroot.gsi.de
[13] V. Toneev, K. Gudima, Phys. A. **400**, 173 (1983)
[14] N. Amelin, K. Gudima, V. Toneev, Sov. J. of Nucl. Phys. **51**, 1093 (1990)
[15] N. Amelin, L. Bravina, L. Csernai, V. Toneev, K. Gudima, S. Sivoklokov, Phys. Rev. C. **47**, 2299 (1993)
[16] K. Gudima, S. Mashnik, A. Sierk, LANL Report LA-UR01-6804 (2001)
[17] http://mpd.jinr.ru
[18] http://garfieldpp.web.cern.ch/garfieldpp/